An Evaluation of Snow Processes for Land Surface Modelling

J.W. POMEROY[1], D.M. GRAY[2], K.R. SHOOK[2], B. TOTH[2],
R.L.H. ESSERY[2], A. PIETRONIRO[1], AND N. HEDSTROM[1]

ABSTRACT

This paper discusses the development and testing of snow algorithms with specific reference to their use and application in land surface models. New algorithms for estimating snow interception in forest canopies, blowing snow transport and sublimation, snowcover depletion and open environment snowmelt are compared to field measurements. Existing algorithms are discussed and compared to field observations. Recommendations are made in respect to:

(a) density of new and aged snow in open and forest environments,
(b) interception of snow by evergreen canopies,
(c) redistribution and sublimation of snow water equivalent by blowing snow,
(d) depletion in snow-covered area during snowmelt,
(e) albedo decay during snowmelt,
(f) turbulent transfer during snowmelt, and
(g) soil heat flux during meltwater infiltration into frozen soils.

Preliminary evidence is presented, suggesting that one relatively advanced land surface model, CLASS, significantly underestimates the timing of snowmelt and snowmelt rates in open environments despite overestimating radiation and turbulent contributions to melt. The cause(s) may be due to overestimation of ground heat loss and other factors. It is recommended that further studies of snow energetics and soil heat transfer in frozen soils be undertaken to provide improvements for land surface models such as CLASS, with particular attention paid to establishing the reliability of the models in invoking closure of the energy equation.

Key words: snow hydrology, general circulation models, CLASS, land surface schemes, energy balance.

INTRODUCTION

Algorithms that describe snow processes are important components of land surface schemes for Global Circulation Models (GCM) because much of the Earth's land surface is covered with snow and ice and strong snow-climate feedbacks have been identified from model output (Cess et al. 1991, Randall et al. 1994, Thomas and Rowntree 1992) and measurements (Karl et al. 1994). Land surface models have been used as the surface interface for GCM and are proposed as the modelling interface between the hydrological and atmospheric systems in coupled atmospheric/hydrological models. As the demand for more sophisticated and physically realistic land surface models increases so does the need to assess current algorithms and recommend the next phase of improvements. The objectives of this paper are to examine several snow processes that are important in the prairie, boreal forest and arctic environments, to evaluate popular algorithms describing these processes, particularly in one relatively advanced model, the Canadian Land Surface Scheme, CLASS (Verseghy 1991, Verseghy et al. 1993) and to recommend new process-based algorithms where applicable. Whilst a selection of the many other models are referred to (e.g. Simple Biosphere Model, SiB, Sellers et al. 1996, Max-Planck-Institut, MPI, Loth et al. 1993, European Centre for Medium-Range Weather Forecast, between Soil, Biosphere and Atmosphere, ISBA, Douville et al. 1995, United Kingdom

[1] National Hydrology Research Centre, 11 Innovation Blvd., Saskatoon, Saskatchewan, S7N 3H5 Canada
[2] Division of Hydrology, University of Saskatchewan, Saskatoon, Saskatchewan, S7N 0W0 Canada

Meteorological Office, UKMO, Essery 1997 National Center for Atmospheric Research, NCAR, Marshall and Oglesby 1994), CLASS algorithms are selected for attention because they treat snow processes in a comprehensive manner compared to many other land surface schemes and they should be expected to work well in Canadian environments.

The snow processes considered here include:

(a) snow interception by forest canopies,
(b) snow redistribution and sublimation by blowing snow,
(c) snow densification and depth variability,
(d) depletion in snow-covered area during ablation,
(e) decay in the albedo of patchy snowcovers during melt, and
(f) melting of complete snowcovers.

Comparisons are made of process-based algorithms, land surface scheme algorithms, and model diagnostic output with field data collected in northern prairie, arctic and southern boreal forest environments. To illustrate the difficulty in evaluating improvements to complex snow models, the changes to CLASS snow calculations that occur when a new process algorithm is coded into CLASS 2.6 are demonstrated.

EXPERIMENTAL SITES AND DATA COLLECTION

Sites

Sites for data collection were chosen in the prairie (Bad Lake/Saskatoon), boreal forest (Waskesiu) and arctic (Trail Valley) regions of western and northern Canada. All locations experience severe continental climates with winter temperatures ranging from just above 0°C down to approximately -40°C and relatively-low annual snowfall. The mean corrected annual snowfall totals (in terms of water equivalent) at the three sites are of the order of: Bad Lake/Saskatoon -- 120 mm, Waskesiu -- 150 mm, and Trail Valley -- 170 mm.

Bad Lake, Saskatchewan: Creighton Watershed, Smith Tributary

The Bad Lake Watershed (51°23'N, 108°26'W, 650 masl.) in south-western Saskatchewan was established as a Research Basin under the International Hydrological Decade Program and instrumented for hydrological research beginning in the late 1960s. The basin is largely cultivated (≈70% of the area) in the production of cereal grains, pulse and legumes by dryland farming. Of the remaining area, 20% is rangeland and 10% is native shrub, grass and farmyards. The topography of the basin ranges from poorly-drained, level plains to moderately and steeply-rolling upland areas, such as the Creighton and Smith Tributaries, which contain deeply-incised channels. Its climate is semi-arid and typical of northern grasslands, with dry, cold winters and hot summers. Snowcovers on the basin exhibit high seasonal and interannual variability. In high snow years, the snowcover normally forms in November and disappears in April, in years with light snows the snowcover forms and ablates several times over the winter with final ablation in March. During low snow years, the major accumulations are found in waterways and within and surrounding windbreaks due to redistribution of the snowfall by wind. Experiments to measure snow-covered area, small-scale and large scale albedo and surface energy balance were conducted during snowmelt periods on 1972 and 1973 (O'Neill 1972, O'Neill and Gray 1973). In 1973 and 1974 extensive snow surveys were conducted over various landscape types during mid-winter and during the snowmelt period (Steppuhn and Dyck 1974).

Saskatoon, Saskatchewan: Kernen Farm

The Kernen Farm located just east of the city of Saskatoon, SK (52°N, 107°W, 500 masl) is an experimental research farm operated by the University of Saskatchewan. It is situated on a flat, open, lacustrine plain, which is cropped to cereal grains and pulse crops under dryland farming. The climate of the area is sub-humid and typical of the northern prairie-parkland transition with cold winters and a snowcover from November through March/April. Experiments were conducted in March 1994 and 1996 on fallow and stubble fields on snow accumulation, snowcover depletion, areal albedo, and the energetics of snowmelt (Shook 1995, Shook and Gray 1997).

Waskesiu, Saskatchewan: Beartrap Creek

The Beartrap Creek basin (53.9°N, 106.1°W, 550 masl), is located near Waskesiu, SK within Prince Albert National Park. Sites in this basin were instrumented in 1992 for a series of forest hydrological process experiments for the Canadian GEWEX and Prince Albert Model Forest studies. The region is dominated by mixed-wood southern boreal forest. Its climate is continental boreal with cold winters and snowcover from late October through April (Harding and Pomeroy 1996, Pomeroy and Dion 1996, Pomeroy et al. 1997a).

Experiments were conducted from a tower in a mature jack pine, Pinus banksia, stand in the

Beartrap Creek. The site is level, has a winter leaf + stem area index of 2.2 m^2/m^2, canopy coverage of 82% and an average tree height of 19 ± 3 m. Over the period of study from November 1994 to April 1995, the low-lying carpet of sphagnum moss and kinnikinnick (bearberry) was covered by snow.

Inuvik, Northwest Territories: Trail Valley Creek

The Trail Valley Creek basin (68°45'N, 133°30'W, 150 masl), located 50 km north of Inuvik, was instrumented for hydrological process and basin modelling experiments in 1991. Currently, these studies form part of the Canadian GEWEX program. The basin has a low arctic climate with snow-cover from September through May. Vegetation is predominately tundra (70%) that is interspersed with large areas of shrub tundra (21%) and small pockets of transitional forest-tundra (1%) (Marsh and Pomeroy 1996). Deep snow drifts, which accumulate in the lee of abrupt changes in topography, cover about 8% of the basin (Pomeroy et al. 1997b). Experiments were conducted using observations of micrometeorological variables made from a tower located on a tundra plain with excellent open, uniform fetch characteristics.

Methodology

Meteorological Stations

At Waskesiu, a variety of meteorological instruments were mounted on the 27-m tower in the centre of the pine stand (Pomeroy et al. 1997a). Parameters used to run CLASS (radiation, air temperature, humidity, wind speed) were measured above the forest canopy. At the top of the tower, two "Kipp and Zonen" shortwave radiometers and one "Middleton" net radiometer measured the incoming and reflected shortwave radiation and net radiation respectively. The radiometers were cleaned weekly and often more frequently when snowfall occurred. Air temperature/humidity was measured using a "Vaisala" HMP35CF hygrothermometer and wind speed was measured using a "Weathertronics" cup anemometer. In addition, the ground heat flux was measured using REBS heat flux plates and snow and soil temperatures were measured using "Type-E" thermocouples. Campbell 21x microloggers were used to control instruments and record data.

At Saskatoon and Trail Valley Creek, 3-m towers were erected in large, uniform, open, snow-covered plains. Similar equipment to that used at Waskesiu was deployed along with an eddy correlation system at Saskatoon. This system comprised a "Solent" ultrasonic anemometer and a "Campbell Scientific" Krypton fast hygrometer. Instantaneous measurements of vertical wind speed, air temperature and specific humidity were made at 10 Hz and covariance calculated over 15 minutes. The eddy correlation system and all other equipment were controlled and logged by Campbell 21x microloggers (Shook and Gray 1997).

At Bad Lake, similar radiation equipment was employed along with standard meteorological equipment used in a climatological station operated by the Atmospheric Environment Service, Environment Canada (Gray and Granger 1988). Snow depth and soil temperatures were also monitored.

Snow Fall, Accumulation and Interception

Snowfall measurements were made with Nipher-shielded AES-style cylinders emptied daily (Bad Lake) or weekly (Waskesiu) or as necessary (Inuvik). The readings were corrected by procedures described by Goodison et al., (1997). At Waskesiu, one-half-hour estimates of snowfall rate were made using a snow particle detector (Brown and Pomeroy 1989), whose counts were given a mass based on weekly snowfall. Snow accumulation was determined from areal snow surveys following the recommendations listed by Pomeroy and Gray (1995). 10-point snow surveys under the pine canopy were used in Waskesiu, whilst longer (+100 point) surveys were used in open environments.

Interception was determined from the difference between snowfall and sub-canopy snowfall or from the weight of snow on a suspended pine tree weighed with a load cell (Hedstrom and Pomeroy 1998). To provide areal averages of snowfall, sub-canopy snowfall was compared to the accumulations determined by snow survey during cold periods and adjusted to provide an areal indicator of sub-canopy snowfall. The difference between snowfall and areally-averaged sub-canopy snowfall was related to the weight of snow on the suspended tree just after new snow events. The ratio of the difference to weight was used to estimate the canopy snow interception load in mm snow water equivalent.

SNOWMELT ACCUMULATION PROCESSES

Snow Interception

Interception by forest canopies can store up to 60% of cumulative snowfall by midwinter in cold boreal forests, which results in a 30%-40% annual loss of snowcover over the winter in many coniferous forest environments (Pomeroy and Gray 1995). Following interception, most snow remains in

the canopy where it is exposed to a relatively warm and dry atmosphere (Lundberg and Halldin 1994). As a result, relatively high rates of sublimation occur from intercepted snow, and more snow sublimates than eventually unloads to the surface (Pomeroy and Schmidt 1993, Pomeroy and Gray 1995, Harding and Pomeroy 1996). In order to calculate the amount of sublimation from intercepted snow, it is important to know the amount of snow collected in the canopy so that appropriate exposure times can be determined. For example, given a constant sublimation rate, an underestimation of interception will result in a shorter exposure time for sublimation and a decrease in seasonal sublimation.

Most land surface schemes do not separate canopy snow from surface snow. CLASS and SiB do consider canopy snow load, but consider the snow interception process in a similar manner to rainfall interception. For instance, CLASS calculates snow interception as a linear function of snowfall, with a maximum intercepted snow depth (kg/m^2) equal to 0.2 LAI, where LAI is the leaf area index (m^2/m^2).

Field data on snow interception collected for a pine forest in Beartrap Creek, Saskatchewan is shown in Fig. 1. Interception measured by nipher-shielded snow gauges is determined as the difference between weekly above- and below-canopy snowfall for periods when there were no major releases or unloading of intercepted snow. Interception measured via a weighed tree is determined by the increase in weight of snow on a suspended tree, expressed as an areal average snow water equivalent, SWE. It is seen that as much as 9 mm SWE can be intercepted in this canopy and that interception increases with snowfall up to snowfall amounts of about 16 mm SWE, above which interception does not increase further. CLASS-modelled interception for such a stand would reach a maximum of 0.44 kg/m^2, more than an order of magnitude less than measured interception

The CLASS snow interception routines produce results that are at odds with measured interception for snowfall events larger than about 3 mm snow water equivalent (SWE[1]). As a result, daily snow accumulation fluxes in coniferous forests are misrepresented. To remedy this situation the following snow interception routine, which is a simplification of that developed by Hedstrom and

[1] Snow Water Equivalent or SWE is expressed as mm of equivalent water per unit area or alternatively as kg/m^2 of snow.

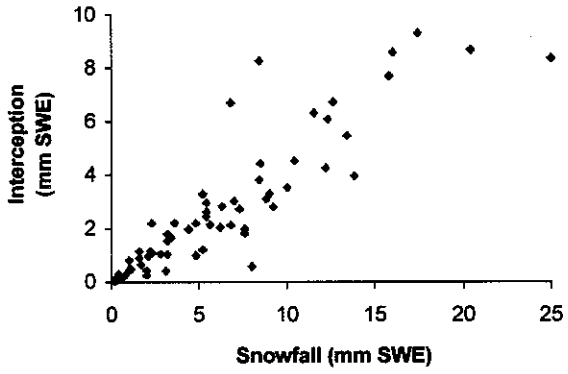

Figure 1. Snow interception of a jack pine canopy at Waskesiu, Sask., measured using the difference in above and below canopy snowfall, converted to areal SWE using snow survey measurements (Hedstrom and Pomeroy, 1998).

Pomeroy (1998), is recommended. The routine is consistent with field observations that snow interception efficiency decreases with snow canopy load and snowfall amount and increases with canopy density (Pomeroy and Gray 1995, Hedstrom and Pomeroy 1998). Modelling this behaviour provides interception, I (kg/m^2), as a function of a dimensionless snow unloading coefficient, c, the difference of the maximum snow load, I*, and initial snow load, I_o (kg/m^2), an exponential function of snowfall, P (kg/m^2 for a unit time), and the canopy density, C_c (proportional coverage) as (Hedstrom and Pomeroy 1998):

$$I = c(I^* - I_o)(1 - e^{-\frac{C_c P}{I^*}}). \qquad (1)$$

This expression is independent of time step except for the unloading coefficient, c. Empirical evidence suggests a value of c = 0.7 is appropriate for hourly time steps. I* is found as a function of LAI (m^2/m^2), a tree species coefficient, S_p (kg/m^2) and fresh snow density, ρ_s (kg/m^3) following Hedstrom and Pomeroy (1998):

$$I^* = S_p LAI(0.27 + \frac{46}{\rho_s}) \qquad (2)$$

Schmidt and Gluns (1991) present field measurements that suggest values for S_p of 6.6 for pine and 5.9 kg/m^2 for spruce. The values for coefficients and constants in Eq. 2 are empirically-derived and hence based on the units expressed above.

The process-based snow interception routine specifies increasing interception efficiency with LAI and decreasing efficiency with increasing snowfall and initial interception as shown in Fig. 2 for a pine canopy. A comparison of modelled and measured snow interception (Fig. 3) shows that this is in agreement with the observed behaviour of snow interception in boreal forest environments.

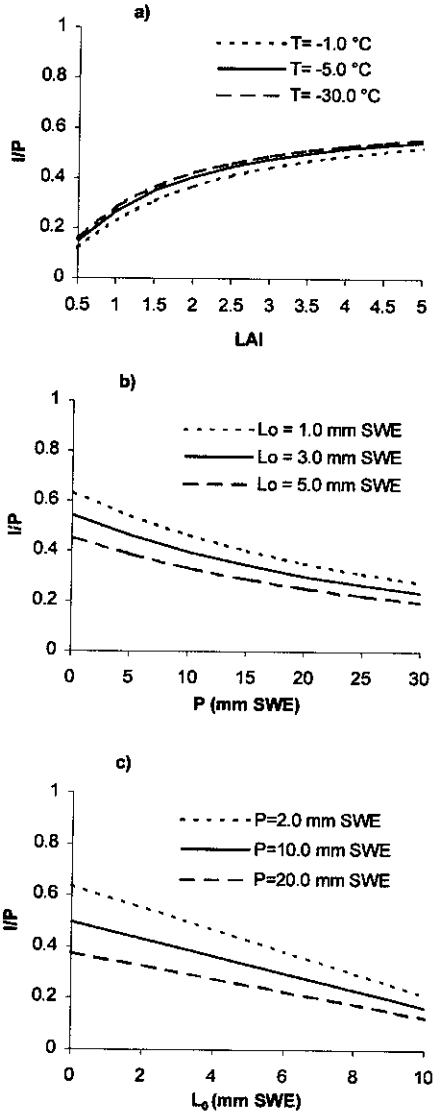

Figure 2. Performance of the process-based snow interception model for ranges of:
a) leaf area index,
b) snowfall, and
c) initial snow load.

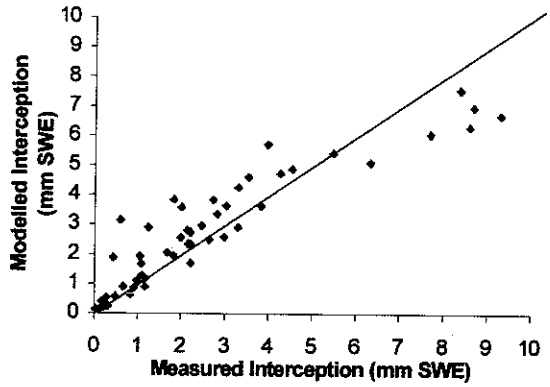

Figure 3. Measured and modelled snow interception. Comparison of the measurements from above and below canopy snowfall gauges, scaled-up using snow surveys and the results of the interception model for Beartrap Creek, 1993 to 1996.

Blowing Snow

Redistribution of snow by wind relocates snow covers and produces notable intransit sublimation of blowing snow (Dyunin 1959, Schmidt 1972, Pomeroy 1989). Relocation may be considered a horizontal mass flux analogous to advection and sublimation considered a vertical flux of water vapour. At the large spatial scales of GCM grid cells, sublimation is the most important blowing snow flux, though transport strongly affects sub-grid variability in snow accumulation. Reported annual fluxes of blowing snow sublimation range from 15% to over 40% (depending on climate, fetch and land use) of annual snowfall on the Canadian Prairies (Pomeroy et al. 1993, Pomeroy and Gray 1995), 28% of annual snowfall on tundra in the Western Canadian Arctic (Pomeroy et al. 1997b) and 32% of annual snowfall on the Alaska north slope (Benson 1982). Blowing-snow sublimation rates are higher than those expected for stationary snow because of the great exposure and ventilation that the snow crystals undergo when lifted by the wind and blown downfield (Dyunin 1959, Schmidt 1972, Pomeroy 1989).

Land surface schemes do not incorporate blowing snow processes. This deficiency can result in appreciable errors in calculations of snow accumulation for open environments. For instance, in the Trail Valley Creek tundra basin in the western Canadian Arctic, Pomeroy et al. (1997b) measured an October through May snowfall of 190 mm SWE. The area is not subject to winter melting and has cold winter air temperatures with minimal surface snow evaporation. In May 1997, the maximum

seasonal accumulations of snow water by landscape type were 68 mm on tundra, 252 mm on shrub tundra and 617 mm in drift areas (steep slopes). Similar magnitudes of difference between snow accumulation and snowfall are noted in the Canadian Prairies, though coupled blowing snow and snowmelt calculations are required to identify the causal factors because of the more variable winter climate of the region (Pomeroy and Li 1997).

The Prairie Blowing Snow Model (PBSM) (Pomeroy 1989, Pomeroy et al. 1993) has been redeveloped for compatibility with GCMs, incorporating features for independent determination of the transport threshold for drifting (Li and Pomeroy 1997a), upscaling blowing snow fluxes using probability theory (Li and Pomeroy 1997b), improved vegetation parameterizations, simplified calculations for variable fetches and landscape-based snow mass balances that include snowmelt (Pomeroy et al. 1997b, Pomeroy and Li 1997). PBSM simulations for fallow and gully land surfaces, along with the results of extensive landscape-based snow surveys for the Bad Lake basin in 1974 are shown in Fig. 4. The relative agreement in both fallow-field (transport-out and sublimation dominated) and gully (transport-in dominated) landscapes suggests that both the small-scale and large-scale snow mass balances can be simulated by a blowing snow model of this type (transport out of fallow must equal transport into gully and accumulation at either site must also balance any sublimation present). The seasonal sublimation and transport losses over the fallow field were 24% and 15% of annual snowfall presuming a fetch of 1-km, had the fetch been 3-km the sublimation loss would have been 1.5 times this value, i.e., 36%. In the gully, the increases in snow accumulation due to blowing snow transport ranged from 50% to 100% of cumulative snowfall. The data from the Arctic and Prairie environments illustrate the need to incorporate blowing snow routines into CLASS for more accurate grid- and sub-grid scale representations of seasonal snow accumulation and sublimation.

Snow Densification

Snow density estimates are important for determining snow depth (when water equivalent is known), heat capacity, thermal conductivity and radiation extinction. Many land surface schemes either assume an average snow density of 250 kg/m^3 (e.g. UKMO, Essery 1997) or calculate average snow density, assuming a density for fresh snow of

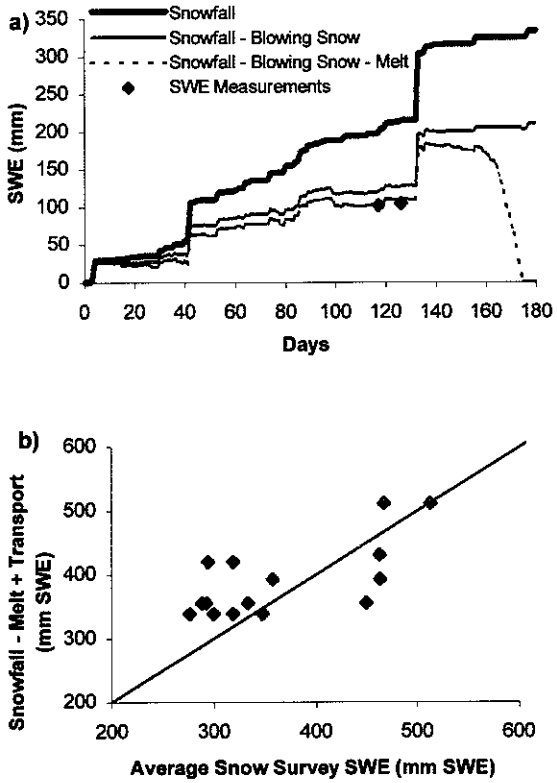

Figure 4. Snow accumulation modelled and SWE measured from extensive snow surveys for
a) open field of fallow at Bad Lake, SK, 1973-1974 and
b) steep shrub-covered slopes at Creighton Watershed, Sask., 1974 using PBSM.

100 kg/m^3 and an exponential increase in density with time up to a maximum value (e.g. CLASS, Verseghy et al. 1993, ISBA, Douville et al. 1995). Important for these simulations are appropriate initial snowfall densities, mechanisms for density increase after deposition and appropriate maximum snow densities.

Contrary to the assumption of constant new snowfall density equal to 100 kg/m^3, the average density of new-fallen snow can vary widely, but for most parts of Canada, has been found to fall in a range between 50 and 120 kg/m^3. Lower values are found during cold, dry conditions and higher values are found in wet snow formed at warm temperatures (Pomeroy and Gray 1995). Rather than a constant value, it is recommended that the algorithm developed by Hedstrom and Pomeroy (1998) be used to calculate the density of fresh snow, ρ_s(fresh) as a function of air temperature. This algorithm, which is based on extensive measurements by the

US Army Corps of Engineers (1956) and Schmidt and Gluns(1991), is:

$$\rho_s(fresh) = 67.9 + 51.3e^{(\frac{T}{2.6})} \quad (3)$$

where T is the air temperature in °C. The algorithm provides for a rapid decrease in fresh snow density as temperature declines from 0 to –12 C and little further decrease for colder temperatures.

Following deposition, the density of new snow increases rapidly, however the rate of increase depends on the processes causing the increase, e.g. crystal metamorphism in the snowpack, crystal settlement, melt and wind packing. Examples of density increases due to wind packing and crystal settlement after wind packing show dramatic, episodic increases. Goodison et al. (1981) measured rates of snow density increase of 8-13 kg/m^3 · h during snowstorms in Ontario (up to 12 h) and approximately 7 kg/m^3 · h immediately after snowfall (up to 6 h) in conditions without blowing snow or melting. Gray et al. (1970) found that density for cold prairie snowpacks increased at approximately 9 kg/m^3 · h during blowing snow storms (up to 24 h). For well-exposed snow in areas subject to snow storms and blowing snow it is appropriate to model episodic increases in density. For non-melting snow in open areas and hourly wind speeds greater than 7 m/s, it is recommended that snow density increase at a rate of 9 kg/m^3 · h during the wind event, up to a maximum that is controlled by snow depth.

Various curves describing the seasonal increase in mean snow density in different environments are reported by Gray and Prowse (1993). These may be used to estimate the density increase due to metamorphism which is the primary mechanism in cold sheltered environments. For many sheltered environments (boreal forest, mountains), relatively slow density increases of the order of 25 kg/m^3 · month are evident during the cold late-winter (Feb.-March). Snowmelt causes rapid increases in density with strong diurnal variation. Melting snow densities range between 350 and 500 kg/m^3 with lower values in morning and higher values later in the day as meltwater is generated a snowcover is primed (Pomeroy and Gray 1995).

The association between maximum cold snow density and depth has been examined in detail by Shook and Gray (1994) from 2400 measurements in the Canadian Prairies. For shallow, aged, wind-blown snow (mean depth, d ≤ 60 cm) there is small covariance between depth and density and the mean density can be taken as 250 kg/m^3 (Shook and Gray 1994). For deeper snow (d > 60 cm), there is a covariance between depth and density and the measurements of Shook and Gray can be used to modify an expression for density given by Tabler et al. (1990), which is based on extensive field measurements of the densities of snow drifts in Wyoming, USA. The form of the expression that matches density measurements on the Canadian prairies is:

$$\rho_s = 450 - \frac{20470}{d}\left[1 - e^{\frac{-d}{67.3}}\right], \quad (4)$$

in which ρ_s is the mean snow density (kg/m^3) corresponding to mean snow depth (d, cm). Equation 4 gives the mean density for aged, windblown snow, providing a maximum value for a non-melted snowcover in an open environment.

In forested and sheltered environments, the episodic density increase with snowfall is not apparent. However, maximum dry snow densities for forested (boreal, mountain forest, maritime) environments with shallow (depth < 1 m) snow reach a maximum value equal to about 250 kg/m^3 (Gray and Prowse 1993). Equation 4 can be used to set a maximum snow density for deep mountain snowpacks that settle due to the weight of snow, as the derivation of the expression included observations taken in coastal mountain environments.

Spatial Variation in Water Equivalent

The small-scale, spatial variation of the snow water equivalent, SWE, within a landscape type is well-recognised and before melt begins is due to wind redistribution of snow and the release of intercepted snow. Knowledge of this variation is especially important for calculating the snow-covered area at various stages of ablation, as explained in the next section of this paper. The spatial variation in SWE in forest environments is primarily due to variations in winter leaf area (up to 70% - Pomeroy and Goodison 1997) and proximity to individual trees (up to 40% - Woo and Steer 1986, Jones 1987, Sturm 1992). In open environments, spatial variations in SWE are due to wind exposure, topography and vegetation. Gray and others (1979) show SWE on brush-covered hillslopes over 10 times greater than that on bare soil hilltops in a prairie environment.

Table 1 lists representative, average values for the coefficient of variation (CV) of SWE that have been

calculated from thousands of samples monitored in seasonal snowcovers near the time of peak accumulation on various landscapes in prairie, arctic and boreal forest environments. The trends exhibited by these data are consistent with the findings reported in the literature (e.g., Woo and Marsh 1977, Pomeroy et al. 1997b) and field observations, such as:

1. The variability in SWE on land with a taller vegetative cover is generally lower. Vegetation dampens the variability in water equivalent due to landform. The denser the vegetation, the greater the effect. However, because of snow interception, evergreen forests produce a greater variability than do deciduous forests.

2. Snow accumulation patterns are affected by those topographic features that cause major divergence in air flow patterns, therefore in snow erosion and deposition. This is evident in the larger values of the coefficient of variation for the crests of hills and the lee of abrupt slopes.

Estimates of CV determined by direct field measurement may vary appreciably around the values listed in Table 1 because:

(a) landscape classification is qualitative and subjective,

(b) land use and landform features are not mutually independent,

Table 1. Representative values for the coefficient of variation of water equivalent of snowcovers, CV, on various landscapes in Prairie, Arctic and Boreal forest environments in late winter.

REGION	*LANDUSE and VEGETATION*	*LANDFORM*	*CV*
PRAIRIES	Fallow	Flat plains; Slightly to moderately rolling topography with gentle slopes	0.47
		Bottom (bed) of wide waterways; Large sloughs and depressions	0.30
		Crests of hills, knolls, and ridges	0.58
	Stubble	All Landforms	0.33
	Pasture	Flat Plains; Bottom (bed) of wide waterways; Large sloughs and depressions; Slightly to moderately rolling topography with gentle slopes	0.41
		Crests of hills, knolls, and ridges	0.51
		Lee of abrupt, sharp slopes	0.57
	Scattered Brush	Bottom (bed) of waterways, e.g., gullies; Sloughs and depressions	0.42
		Lee of abrupt sharp, slopes	0.52
	Treed Farm Yards		0.50
ARCTIC	Tundra	Flat plains, upland plateaux, slight to moderately rolling topography	0.31
		Valley bottoms	0.28
		Valley sides (drifts where slopes greater than 9°)	0.34
	Shrub Tundra	Flat plains, slight to moderately rolling topography	0.22
		Valley bottoms	0.16
		Valley sides (drifts where slopes greater than 9°)	0.18
	Sparse	Exposed hillside and forest edge	0.21
	Forest-tundra	Sheltered	0.11
BOREAL FOREST	Black Spruce		0.14
	Mature Jack Pine		0.10
	Mixed Aspen-White Spruce	All Landforms	0.05
	Young Jack Pine		0.14
	Recent Clear-cut		0.07
	Recent Burn		0.04

(c) CV will vary with factors other than landscape features, e.g., with differences in processes affecting snow metamorphism, snowfall distribution, redistribution of snow by wind, interception and sample size. Many of the processes that cause redistribution affect the standard deviation and mean of SWE quite differently, and
(d) interannual changes in mean SWE associated with variable snowfall may alter the CV even with little change in processes that lead to the net redistribution flux.

SNOWMELT PROCESSES

The snowmelt period is one of rapid changes in land-atmosphere exchange as albedo, turbulent fluxes, internal snow energy and surface temperature undergo dramatic alteration as the snowcover becomes wet and then is depleted. Hydrology is also strongly affected as snowmelt water flows through the pack, either infiltrates, evaporates or provides the spring freshet. In many northern environments the spring freshet is the largest annual runoff event, comprising approximately 50%, 90% and 70% of annual flow for boreal forest, prairie and arctic environments respectively (Gray 1970, Hetherington 1987, Woo 1990). It is therefore critical for atmospheric and hydrological models to properly determine areal energy fluxes, radiative and turbulent exchange with the snowpack, internal energy changes and energy exchange with the ground during the melt period. This section examines the change in snow-covered area during melt and melt energetics.

Snowcover Depletion

Most snowcovers disintegrate into a mosaic of patches of snow and "bare" ground as they ablate. This disintegration affects the geometry and area of snowcover, which affect the energetics of the melt process and the contributing areas of melt, runoff, infiltration and soil water recharge. In order to include the effects of the patchiness of a snowcover on these components in snowmelt simulations it is necessary to incorporate in the algorithm a measure of the geometrical character of the snow field during ablation. Most land surface algorithms do not consider the decrease in snow-covered area during snowmelt. CLASS, however, does when the mean depth of snow is $\leq$ 10 cm, the limiting snow depth after which bare patches begin to appear (Donald et al. 1995). It calculates the areal fraction of snowcover, F_s, as:

$$f_{sn} = \frac{W_s}{0.10\rho_s}, \qquad (5)$$

in which W_s is the mass of snow per unit area over the grid (kg/m^2) and ρ_s the snow density (kg/m^3).

Two assumptions used by Eq. 5 conflict with the physics and properties of most natural-ablating snow fields. They are:
(a) areal snowcover depletion starts when the mean snow depth is equal to 10 cm and
(b) the spatial distribution of snow water is uniform.

Shook (1993, 1995) and Shook et al. (1993, 1994) demonstrated that in environments where the melt flux is relatively uniform over an area, the fractal character of the spatial distribution of the water equivalent controls the geometries of the soil and snow patches of an ablating snowcover.

Donald et al. 1995 also showed clearly that snow depth distribution for snowpacks in Southern Ontario followed a three-parameter log-normal distribution. Once the limiting snow depth was reached, the depth distribution followed a two-parameter log-normal probablity density function. Using this function, Donald (1992) derived a simple "melt model" where the theoretical average snow depth and fraction of snow (F_s) curves could be described through a uniform shift (M_a) of the depth distribution. The remaining snow-covered area fraction F_s is given by (Donald et al. 1995):

$$F_s(M_a) = \frac{1}{2} erfc\left(z_{M_a} / \sqrt{2}\right) \qquad (6)$$

where, $z_{M_a} = \left(\frac{\ln M_a - \lambda}{\xi}\right)$;

$$\xi = \sqrt{\ln(1+\sigma^2/\mu^2)};$$

$$\lambda = \ln(\mu) - \tfrac{1}{2}\xi^2;$$

and μ and σ are the mean and the standard deviation of the snow depth at the limiting value and *erfc* is an error function. Note that the definition of λ in Eq. 6 corrects an error in the paper by Donald et al. The corresponding expression for the average depth over the entire area, resulting in the same distribution shift of M_a was solved analytically as (Donald et al. 1995):

$$\overline{D}(M_a) = \frac{1}{2} e^{\lambda + \frac{1}{2}\xi^2} \cdot erfc\left(\frac{1}{\sqrt{2}}\left(z_{M_a} - \xi\right)\right) - M_a \cdot F_s(M_a) \qquad (7)$$

Shook (1995) noted that the spatial frequency distribution of the snow water equivalent (SWE), as opposed to snow depth, of a natural snowcover often can be approximated by the lognormal probability density function which he expressed in linear form as:

$$SWE = \overline{SWE}(1 + KCV), \qquad (8)$$

where the terms are: SWE, snow water equivalent having an exceedance probability equal to that of the frequency factor, K (Chow 1954); $\overline{SWE}$, mean snow water equivalent; and CV, coefficient of variation. Figure 5 plots point measurements of SWE and fitted lognormal distributions for three landscapes in a prairie environment:

(a) a relatively-flat field in wheat stubble,
(b) an undulating field of fallow and
(c) a relatively-flat low area with scattered brush.

The respective coefficients of determination, r^2, between the measured and fitted SWE-values for the landscapes are 0.92, 0.98 and 0.99, respectively.

Shook (1995) also noted that the snowcover-depletion curve is produced by applying the snow melt rate evenly over the SWE frequency distribution. The applied snow melt is designated M_a and represents the total depth of melt at any point in the snowcover. If there is no covariance between depth and density of snowpacks (as is the case for shallow snow) then the algorithm of Donald et al. (1995) can be applied without modification and applied melt is equivalent to the shift in the depth distribution, M_a. However, large-scale models generally consider snow melt to be the volume of meltwater produced per unit area of grid cell. This quantity, which is the result of the application of M_a, is denoted as M, the resultant melt. Therefore, the fraction of snowcover, F_s, must be know to calculate M from M_a. The two quantities are related by:

$$M_r = \int_0^{M_a} F_s \, dM_a \qquad (9)$$

which is the basis for the theoretical development of Eqs. 6 and 7 using SWE rather than depth. Under conditions where the melt flux over an area is approximately uniform, a reasonable representation of the depletion of snow-covered area (F_s) during ablation can be obtained by melting the frequency distribution of SWE or solving directly using Eqs 6 and 7.

The results of this procedure are demonstrated in Fig. 6, which plots the decrease in F_s over time for a constant melt rate, assuming initial conditions of a lognormal distribution of SWE with various CV values. The results show that the smaller the CV, the more rapid the depletion of F_s. This trend is the result of the increased peakedness of the frequency distribution of SWE with decreasing CV. The smaller the CV, the larger the number of SWE-values grouped near to the mean.

The snow-covered area depletion algorithm developed by Shook (1995) was tested using data collected on the Smith Tributary at Bad Lake in 1972, with melt rates driven by a temperature-index model. The results are shown in Fig. 7 and demonstrate reasonable correspondence between modelled and measured areal depletion of snowcover (Shook 1995).

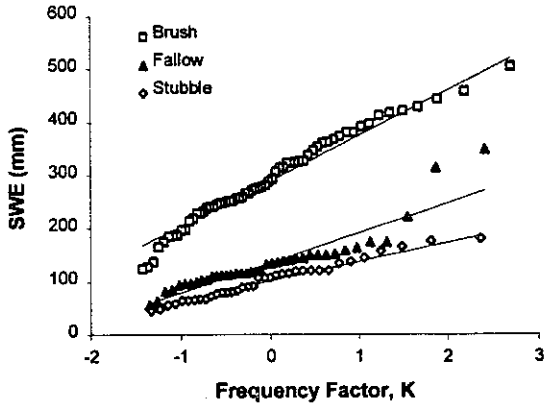

Figure 5. Lognormal distribution fitted to point measurements of SWE taken on open landscapes in brush, fallow and wheat stubble - Smith Tributary, Sask., 1972.

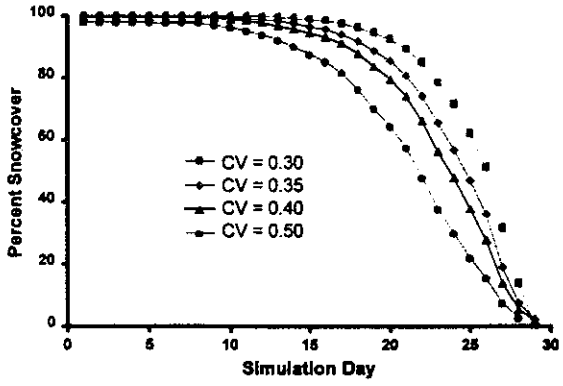

Figure 6. Snow-covered area depletion curves modelled by applying a constant, uniform melt rate to snowcovers whose SWE have a log normal distribution. Fractional snowcover is plotted against time from an initial SWE of 130 mm for various coefficients of variation of SWE, CV.

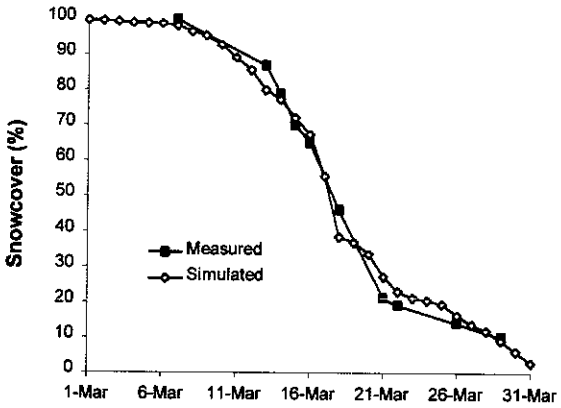

Figure 7. Modelled and measured snowcover depletion curves during snow ablation on the Smith Tributary in 1972.

Snowmelt Energetics

Land surface schemes calculate the energy available for snowmelt, Q_m, by an energy balance equation. Therefore, assuming a continuous snowcover:

$$Q_m + Q_n + Q_h + Q_e + Q_a + Q_g = dU/dt, \quad (10)$$

The terms of Eq. 10 are: Q_n, net radiation, Q_h, turbulent flux of sensible heat exchanged at the surface due to a difference in temperature between the surface and overlying air, Q_e, turbulent flux of latent energy exchanged at the surface due to vapour movement as a result of a difference in vapour pressure between the surface and overlying air, Q_a, energy advected to the snowpack from rainfall or other processes, Q_g, ground heat flux due to conduction, U, internal energy, and t, time. With the exception of Q_a and dU/dt, the various terms in Eq. 10 are examined below with respect to measurements, land surface scheme representations and process algorithms. Discussions of the Q_a term have been recently provided by Marsh et al. (1997), Liston (1995) and Shook (1995), whilst Male (1980) and Marsh and Woo (1994) provided a detailed examination of dU/dt.

Radiation

The radiation balance in land surface schemes is typically composed of long and short-wave terms. The long-wave balance as affected by snow depends on the surface temperature, which is normally solved for by an iterative solution of an energy balance at the surface. Actively melting snow has a surface temperature of 0 C; departures from this value at night depend on snowpack internal and external energetics. Errors in other components of the energy balance can therefore cause errors in the longwave flux.

Short-wave energy fluxes are influenced by the snow albedo. The interaction between vegetation and snow-cover albedo is complex however, even when snow covers vegetation. For instance, Pomeroy and Dion (1996) have shown snow-covered boreal pine canopies act as "light-traps", such that the canopy albedo is unaffected by intercepted snow load. Some land surface schemes correctly simulate this feature (CLASS, SiB, UKMO) but some increase canopy albedo after recent snowfalls (ECMWF, Betts et al. 1996). In shrub-covered clearings of the boreal forest, Pomeroy and Granger (1997) found net radiation during melt became enhanced as low shrub vegetation became exposed, lowering the albedo. For this reason Q_n - Q_g was 2.36 times Q_m over the melt period and turbulent contributions to melt were negligible. For surface snowcovers, most land surface schemes neglect the role of protruding vegetation, but some do reduce the albedo as fresh snow ages, with further modifications during melt (e.g. ISBA, MPI, CLASS). For instance, CLASS assumes an albedo for "fresh" snow of 0.84 to a lower limit of 0.70 for "old snow". The variation in snow albedo, α_{sn}, with time, t (s), is approximated by the expression:

$$\alpha_{sn}(t+1) = [\alpha_{sn}(t) - 0.70 - \exp\left[\frac{-0.01\Delta t}{3600}\right] + 0.70. \quad (11)$$

α_{sn} decreases until a new snowfall event occurs, which returns the albedo to 0.84. The lower limit of 0.7 is decreased further to 0.50 if liquid water is present on top of the snowpack.

Modelling studies such as by Wiscombe and Warren (1980) provide the albedo of complete snowcovers from theoretical principles and have been successfully incorporated in snow models (Marshall and Oglesby 1994). However, it is often difficult to interpret field measurements of areal albedo, α, made with hemispherical radiometers because of the decrease in snow-covered area during melt. Field measurements of albedo can be corrected using measured fractions of snow-covered area, F_s, from aerial photographs to provide estimates of the variation of α_{sn} during melt. For patchy snowcover, the snow albedo, α_{sn}, is obtained from areal albedo by weighting the albedos of snow and ground according to a segregation based on the fraction of the unit area covered by each surface. This

technique is commonly employed by recent land surface schemes to calculate areal albedo during melt, and is:

$$\alpha = \alpha_{sn} f_{in} + \alpha_g (1 - f_{in}), \qquad (12)$$

where α_g = the albedo of snow-free ground.

Shook (1993) demonstrated that the association between α and F_s during snowmelt on the Canadian prairies is approximately linear over a large range in F_s (0.9-0.1), as shown in Fig. 8. A linear association between α and F_s suggests that α_{sn} does not vary greatly during ablation and that the major factor controlling the decay in α is the fraction of bare ground. The upper limit of α is established primarily by α_{sn}, closely following the start of depletion in SCA; the lower limit is set by α_g. Fitting a linear regression to the data for Smith Tributary, Bad Lake, Sask. in Fig. 8 gives an intercept of 0.096 and a slope of 0.75 with a correlation coefficient, r = 0.99. The corresponding values for the albedos of ground and snow by Eq. 12 are therefore $\alpha_g = 0.096$ and $\alpha_{sn} = 0.85$. A similar analyses applied to the measurements for the Creighton sub-basin of Bad Lake gave the corresponding statistics: intercept = 0.095, slope = 0.42, r = 0.95, $\alpha_g = 0.095$ and $\alpha_{sn} = 0.52$. The lower albedo for snow on the Creighton Watershed is due to a shallow, dirty snowcover and vegetation protruding through the snow surface. The large differences in snow albedo between snowcovers of similar grainsize and wetness suggest that much of the variation in albedo with grain size may be overwhelmed by local factors such as dust, pollution and protruding vegetation. These results also suggest that the changes in the reflectance of snow during ablation are small and have little effect on α. The data call into question the presumption in albedo calculations that melting snow is "clean" and covers vegetation during melt. The decrease of α_{sn} to 0.5 for wet snow by CLASS would also appear inappropriate as the field measurements provided no evidence that snow albedo declines during the decrease in snow-covered area.

Ground Heat Flux

Most simulations of ground heat in land surface models are based on heat transfer by conduction using the temperature gradient approach and simulated soil temperatures at three or four levels in a soil profile that extends to the rooting depth of the crop or below. Often, heat transfers due to phase changes from freezing and thawing in frozen soils are either ignored or the freezing point depression

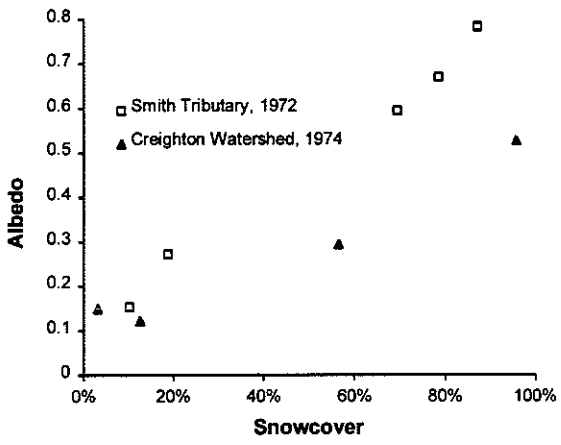

Figure 8. Relation between areal albedo, α_A, and snow-covered area, monitored on two small watersheds at Bad Lake, SK.

relationship - the curve describing the association between liquid water content and freezing temperature - is represented as a step function rather than as a continuous curve.

Impermeable soils.

When water from a melting snowcover is unable to infiltrate a frozen soil, such as may occur when an ice lens has formed on the soil surface or in ice-rich, uncracked permafrost, the temperature gradient method may be expected to give reasonable estimates of the ground heat flux. If the soils are very cold, intense temperature gradients and high fluxes may develop and lead to the formation of basal ice layers at the soil surface (Woo et al. 1982). This refreezing may result in large changes in internal energy of the snowpack (Marsh and Woo 1984).

Permeable soils.

For most northern regions, some infiltration of meltwater into frozen soils accompanies snow ablation. Under these conditions the ground heat flux is usually small compared to the melt energy flux. Average daily ground heat fluxes generally fall in the range from 0 to 4.6 W/m^2. Nevertheless, where algorithms are used to estimate the flux, the component must be calculated correctly because an error in the calculation may affect the determination of the other terms of the energy equation and closure of the energy balance. For example, a poor estimate of snow surface temperature will affect the calculations of albedo, sensible and latent heat in most land surface models.

The application of a temperature-gradient approach for estimating the ground heat flux in frozen soils during snowmelt infiltration is not straightforward. A major reason for the difficulty is that important heat and mass transfer processes affecting the flux occur in the upper portion of the temperature profile. For example, Gray et al. (1985) reported that the average depth of meltwater penetrating frozen agricultural soils of the Canadian Prairies was about 30 cm (standard deviation = ± 10 cm).

Infiltration into frozen ground involves simultaneous coupled heat and mass transfers with phase changes. Field measurements (Kane and Stein 1983) and model simulations (Zhao et. al. 1997) demonstrate that both the infiltration rate and the surface heat transfer rate (conduction) decrease with time following the application of meltwater to the surface (Fig. 9). Zhao et. al. (1997) suggested that these variations may be described by two regimes, a transient regime and a quasi-steady state regime. The transient regime follows immediately the application of water to the soil surface. During this period the infiltration rate and the heat transfer rate decrease rapidly. The quasi-steady state regime develops when the changes in the infiltration rate and the heat transfer rate with time become relatively small. The duration of the transient period is usually short (a few hours), depending on the hydraulic properties of the soil, surface condition, initial water content and initial temperature of the soil. During transient flow, the energy used to increase the soil temperature is largely supplied by heat conduction at the surface (high heat transfer rate at the surface) (Zhao et. al. 1997). In the quasi-steady state regime, the energy used to increase the soil temperature at depth is supplied by latent heat released by the refreezing of percolating meltwater in the soil layers above (low heat transfer rate at the surface.

Figure 10 shows simulated profiles of ice content, θ_i (Fig. 10a), heat flux, dQ/dt (Fig 10b) and soil temperature, T (Fig. 10c) after 2, 8, 12, and 24 h of infiltration into a frozen soil with initial and boundary conditions of: total soil moisture pore saturation = 0.40, soil temperature = -4°C and surface pore saturation = 0.75. Figure 10a shows soil layers with an increase in ice content (freezing) overlying soil layers with a decrease in ice content. Most of the latent heat (say 90%) released by the refreezing of meltwater is conducted deeper in the soil where it used for melting and increasing the soil temperature (Zhao et al. 1997). Figure 10b shows the

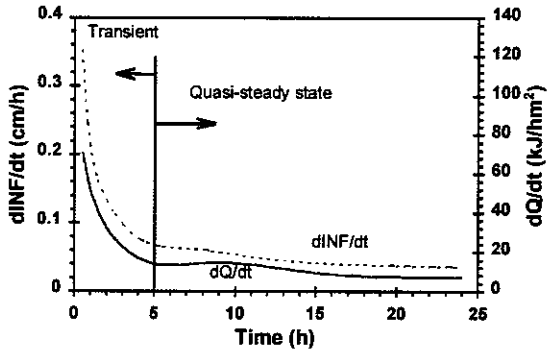

Figure 9. Variations in infiltration rate (dINF/dt) and surface heat flux rate (dQ/dt) with time during snowmelt infiltration into a frozen silty-clay soil.

depth of maximum heat flux coincides with the depth of maximum melting (Fig 10c). The heat flux dampens as the maximum flux moves deeper into the soil. As indicated above, the energy added to a soil by conduction from the surface is only important to the thermal balance during the early stages of infiltration. With increasing time the ground heat flux decreases due to decreases in the temperature gradient in soil layers near the surface (Fig. 10c).

Turbulent Fluxes

The success of determining the melt flux over snow by Eq. 10 can be highly variable, which is often attributed (see Male and Granger 1979) to the difficulties in obtaining accurate, reliable estimates of the convective turbulent fluxes by bulk aerodynamic transfer equations similar to those used in many land surface schemes. Land-surface models parameterise exchanges of heat and moisture between the atmosphere and the surface using relationships of the forms

$$H = \rho \; c_p \; C_H \; U \; \Delta T \qquad (13)$$

and

$$E = \rho \; C_H \; U \; \Delta q, \qquad (14)$$

where ρ_a and C_p are the density and heat capacity of air, h_v is the latent heat of vaporisation, D_h and D_e are exchange coefficients, u is the wind speed at a reference height in the atmosphere, and ΔT and Δq are temperature and humidity differences between the surface and the reference level. The surface humidity is generally assumed to be saturated over snow and the surface temperature cannot rise above

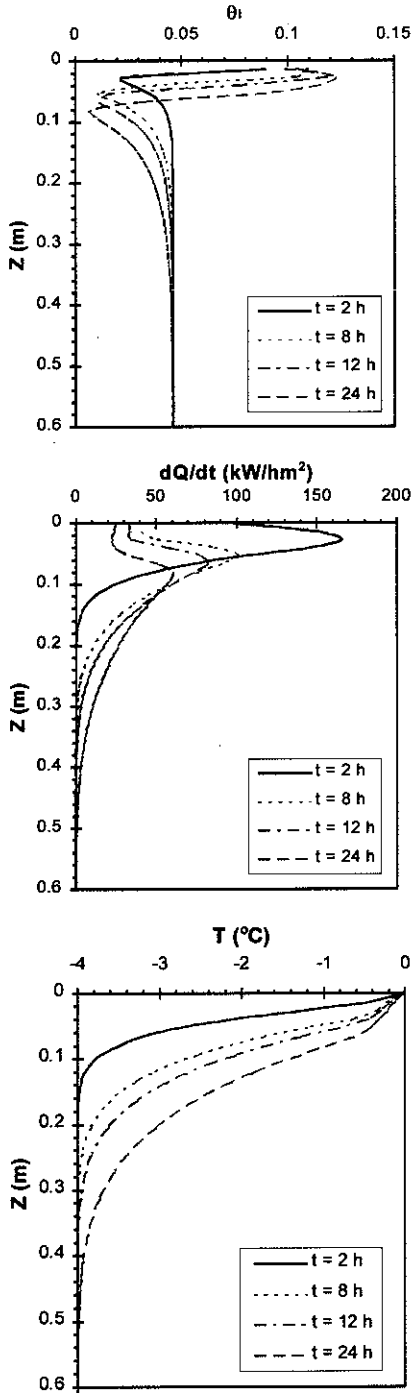

Figure 10. Simulated profiles of variations in:

a) ice content,

b) heat flux, and

c) soil temperature with depth after 2, 8, 12 and 24 h of continuous snowmelt infiltration into a frozen silty-clay soil. Initial and boundary conditions: soil pore saturation = 0.40, surface pore saturation = 0.75 and soil temperature = -4° C.

0°C; snowmelt is diagnosed from the energy required to balance the surface energy budget subject to the surface temperature constraint. Exchange coefficients are calculated as functions of surface roughness and some index of atmospheric stability - either a Monin-Obukhov length or a Richardson number.

Those factors contributing to the difficulties and problems in calculating turbulent exchange in this manner include:

The validity of the assumption of a constant flux layer. de La Casiniere (1974), Granger, (1977) and Halberstram and Schieldge (1981) observed a temperature maximum in the air layer 10–50 cm above the surface of melting snow due to radiation heating. With the upper limit of snow surface temperature at 0 °C, the temperature anomaly results in a stable profile directing heat towards the surface. Therefore, not only is the heat flux not constant with height but it undergoes a reversal in direction at the level of the raised maximum. Expressions that make use of the air temperature at 1–2 m and the temperature of the snow surface, will give a sensible heat flux in the wrong direction.

Typically, snowcovers have low thermal conductivities and high albedos and emissivities and a snow surface can be very cold, especially on cold nights. This results in extremely stable conditions of the atmospheric surface layer that dampen turbulent mixing (Male 1980).

The eddy diffusivities for latent and sensible energy and momentum are not equal (Male and Granger 1979).

Snow and ice are smooth surfaces that lead to low shear velocities and induced levels of turbulence. Yen (1995) estimated the sensible heat flux over snow- or ice-covered ground during the winter months is only about one-third of that over grass-covered ground during spring and summer months.

A comparison of turbulent flux schemes during snowmelt was made for an isothermal, continuous, unvegetated snowpack near Saskatoon on 11 and 12 March 1996 and is shown in Fig. 11. Three schemes were tested: the 'log-linear' form commonly used for stable conditions (Webb 1970), a modification developed by Granger and Male (1978) from measurements over snow, and a Richardson number formulation typical of the type used in large-scale atmospheric models (McFarlane *et al.*, 1992). For comparison, net radiation less ground heat flux is

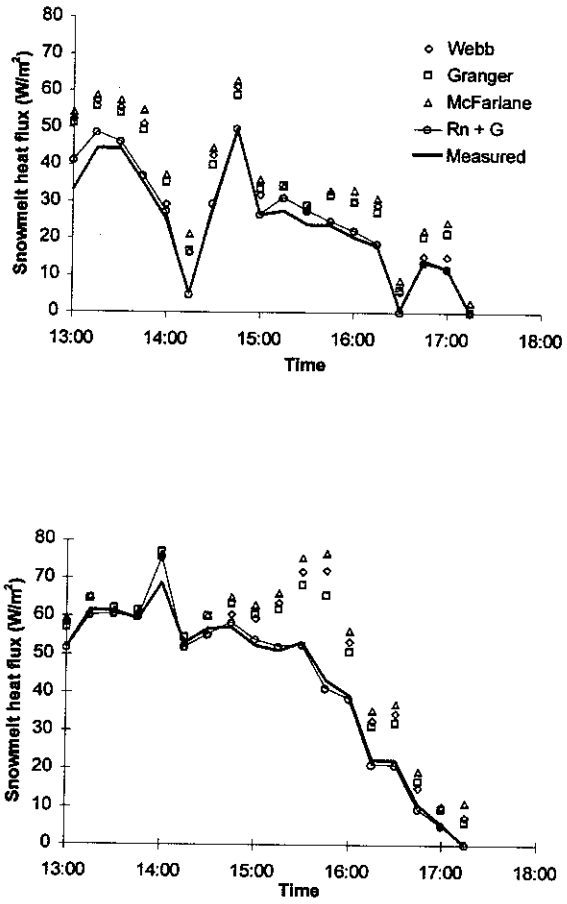

Figure 11. Comparison of snowmelt heat flux measured using the measured inputs to the energy balance equation, and modelled using ground and radiation fluxes and estimated sensible and latent heat fluxes from the following schemes: Webb (1970), Granger and Male (1981) and McFarlane et al. (1992). The net radiation less ground heat flux is shown for further evaluation of the actual contribution from turbulent fluxes.

shown. *All* of the turbulent transfer schemes overestimate the downward (largely sensible) convective energy available for melt, the degree of overestimation depending upon the stability correction employed. RMS errors in estimates of snowmelt heat fluxes over the 13:00 - 17:00 period are shown in Table 2 for both days. Interestingly, the "best" melt rate simulation is obtained by disabling the turbulent transfer schemes and simply using net radiation and ground heat flux to estimate snowmelt.

Table 2. RMS errors (W/m²) during isothermal melt of a continuous open snowcover in estimates of snowmelt heat fluxes by various commonly used turbulent exchange algorithms, compared to net radiation less ground heat flux. Kernan Farm, Saskatoon, Sask 1996.

	Webb	*Granger*	*McFarlane*	$Q_n + Q_g$
March 11	10.0	10.0	13.0	2.8
March 12	10.7	9.0	13.0	2.0

To obtain more reliable and stable estimates of snowmelt, a modified form of the Penman-Monteith expression for estimating evaporation from vegetative surfaces (Monteith 1965, 1981) was developed and tested. This procedure combines the aerodynamic and energy balance approaches to determine the energy available for phase change(s). Shook and Gray (1997) give the expression for the energy available for snowmelt, Q_m, as:

$$Q_m = \frac{k}{1-k}\left[\frac{\Delta\left(Q_n - Q_g\right) + \rho_a C_p \dfrac{\left(e_a^* - e_a\right)}{r_a}}{\Delta\left(\dfrac{k}{1-k}+1\right)+\gamma}\right] \quad (15)$$

where the terms are: k, time-averaged, bulk coefficient equal to the ratio of the energy used for melting to the total energy available for melting + vaporisation; Δ, slope of the saturation vapour pressure-temperature curve, normally taken at the air temperature, T_a, or at $(T_a + T_d)/2$, where T_d is the dew point temperature; Q_n, net radiation; Q_g, ground heat flux; ρ_a, density of air; C_p, specific heat of air; e_a^*, saturation vapour pressure at the air temperature, T_a; e_a, vapour pressure of the air at T_a; r_a, aerodynamic resistance; and γ, pyschrometric constant. For neutral conditions and fully-developed turbulent flow, r_a can be determined from measurements of the wind speed profile in the expression:

$$r_a = \frac{\left(\ln\dfrac{\left(z-d_o\right)}{z_o}\right)^2}{k^2 u_z}, \quad (16)$$

where the terms are: z, height of measurement of wind speed, u_z; d_o, zero plane displacement height; z_o, aerodynamic roughness height, and k, von Karman's constant.

Equation 15 assumes: (a) saturated surface, (b) an isothermal snowpack at 0°C, (c) fully-developed turbulent flow, (d) the horizontal gradients of energy and water vapour flow are zero, and (e) the eddy diffusivities of latent and sensible energy are equal. Therefore, likely it is most applicable for a melting snowcover on long fetches of uniform cover in the presence of stationary or slow-moving, stable, large-scale air masses.

An exact partitioning of the total energy available for the phase change(s) among evaporation and melt would involve solving the coupled heat and mass transfer equations of a system that displays large temporal variation and enormous spatial variability. Therefore, it is assumed that the proportionality between the phase change fluxes can be described by a time-averaged, bulk coefficient, k, such that $k = Q_m/(Q_m + Q_e)$ - the ratio of the energy used for melting to the total energy available for melting + vaporisation. k will vary in magnitude between 0 (all energy is used by evaporation) and 1 (all energy is used for melting).

Shook and Gray (1997) compared the melt fluxes calculated by Eq. 15 with those determined by measurements on two days during the spring of 1996 on the Canadian Prairies under conditions with large-scale advection and warm air aloft. Figure 12 plots these data with k = 0.60, 0.85, 0.90 and 0.98. The results of a linear regression analyses of predicted on measured estimates of Q_m, for these and other values for k are given in Table 3. They suggest that the "true" value of k is likely near 0.98.

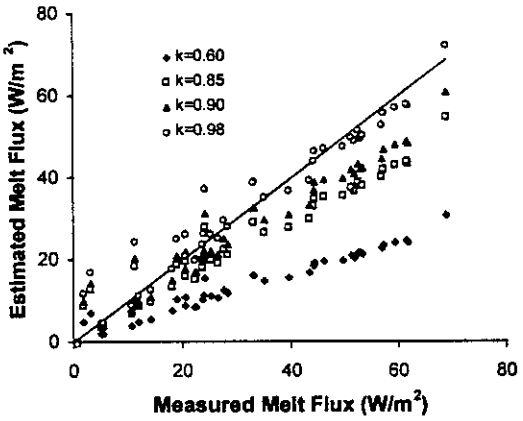

Figure 12. Comparison of 15-min melt fluxes calculated from field energy balance measurements over complete snowcover at Saskatoon, SK with corresponding fluxes calculated by the modified Penman-Monteith expression (Eq. 15) with k = 0.6, k = 0.85, k = 0.90 and k = 0.98.

Model Simulations of Melt

An appreciation of the difficulties of modelling snow melt with even a relatively sophisticated land surface scheme and the limited degree of improvement in performance that can be expected when correcting algorithms of a scheme in isolation is shown in the following section, with respect to CLASS. CLASS was chosen because it contains representation of the phenomenon demonstrated (snow-covered area depletion, energetics of snowmelt, multi-layer soil model) and should be expected to perform well in a major Canadian environment (prairies).

Snow-covered Area Depletion

An attempt was made to examine the effect of incorporating the recommended snow-cover depletion curve in CLASS on performance during ablation on a flat unvegetated field near Saskatoon in 1994 (Fig. 13). The comparisons show that both CLASS and modified CLASS (with the snowcover

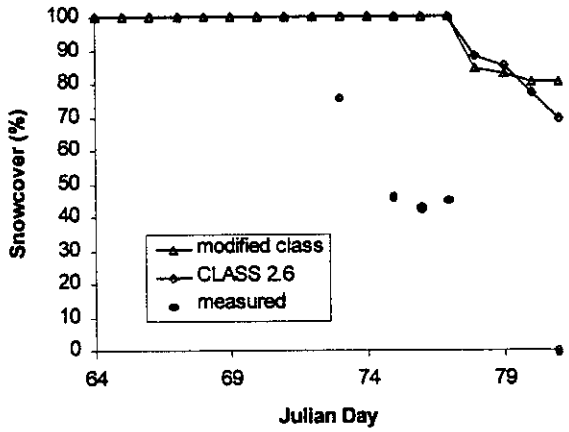

Figure 13. Comparison of CLASS and modified CLASS in predicting snowcover depletion on a flat field of fallow at Kernen Farm, near Saskatoon, March 1994.

Table 3. Linear regressions of estimated on measured Q_m values, for various values of k. Kernen Farm, Saskatoon, March 11 and 12, 1996. r^2 = coefficient of determination.

k	*Slope of Best-fit Line*	r^2
0.60	0.419	0.931
0.85	0.748	0.927
0.90	0.835	0.926
0.95	0.933	0.925
0.98	0.997	0.924
0.99	1.019	0.924

depletion algorithm) are about five days late in the start of snowcover depletion relative to that measured. The delay makes it impossible to assess changes in performance due to the new snow-cover depletion curve. This observation also suggests that the benefits of more physically-realistic snow-covered area depletion cannot be realised without an assessment of the energetics of the CLASS snowmelt routine.

Snowmelt Energetics

Energy flux measurements collected near Saskatoon during March 11-13, 1996 were used to examine the performance of CLASS simulations of the melt of shallow, continuous, open environment snow covers. CLASS was run on an hourly basis using net longwave and incoming shortwave radiation, air temperature, wind speed and dewpoint. Initial snow and soil conditions were determined by field measurements. Figure 14 compares the 30-minute melt fluxes calculated by CLASS with those calculated using measured components in the energy equation (Eq. 10) on March 12, 1996 near Saskatoon. CLASS tends to underestimate the net energy available for melt, with values ranging from 50 to 64 W/m^2 during periods in the afternoon, and averaging 35 W/m^2 over the interval 1230 - 1700. Another important feature demonstrated in Fig. 14 is the delay in timing of melt by CLASS. CLASS does not show melt occurring until 1500 h.

To study the effects of deviations in the modelled estimates of components of the energy equation on the calculation of the melt flux, comparisons between "modelled" and "measured" values were made for the three-day period on the Kernen farm when the measured melt fluxes

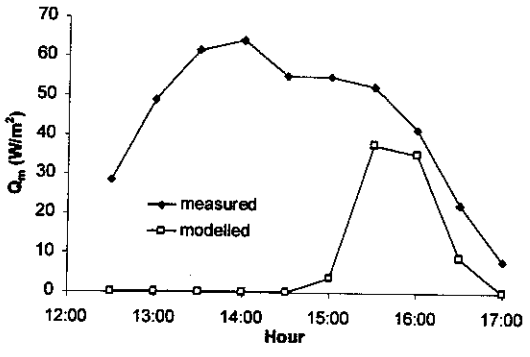

Figure 14. Comparison of 30-min melt fluxes calculated by CLASS and corresponding values determined using measured components in the energy equation, Kernen Farm, near Saskatoon, March 12, 1996.

(determined using measured values in the energy equation) were positive. Figure 15 plots "modelled" versus "measured" 30-min fluxes of: (a) net radiation, (b) latent energy, (b) sensible energy and (d) ground heat for the same time period on March 12,1996 described by Fig. 14.

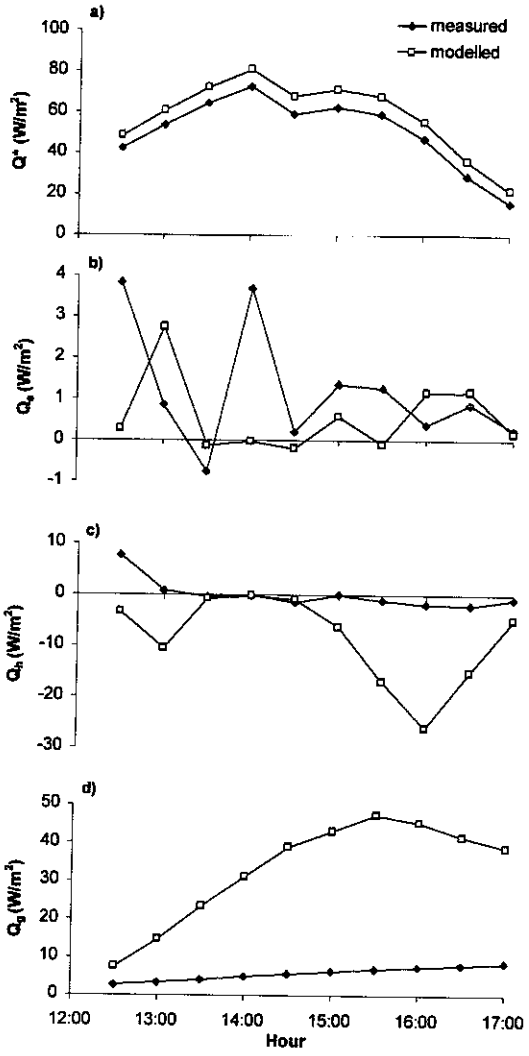

Figure 15. Comparisons of modelled and measured 30-min fluxes at Kernen Farm near Saskatoon during melt on March 12, 1996:

a) net radiation,
b) latent energy,
c) sensible energy, and
d) ground heat.

Note net radiation is positive when directed to the pack, all other fluxes are positive when they are directed away from the pack.

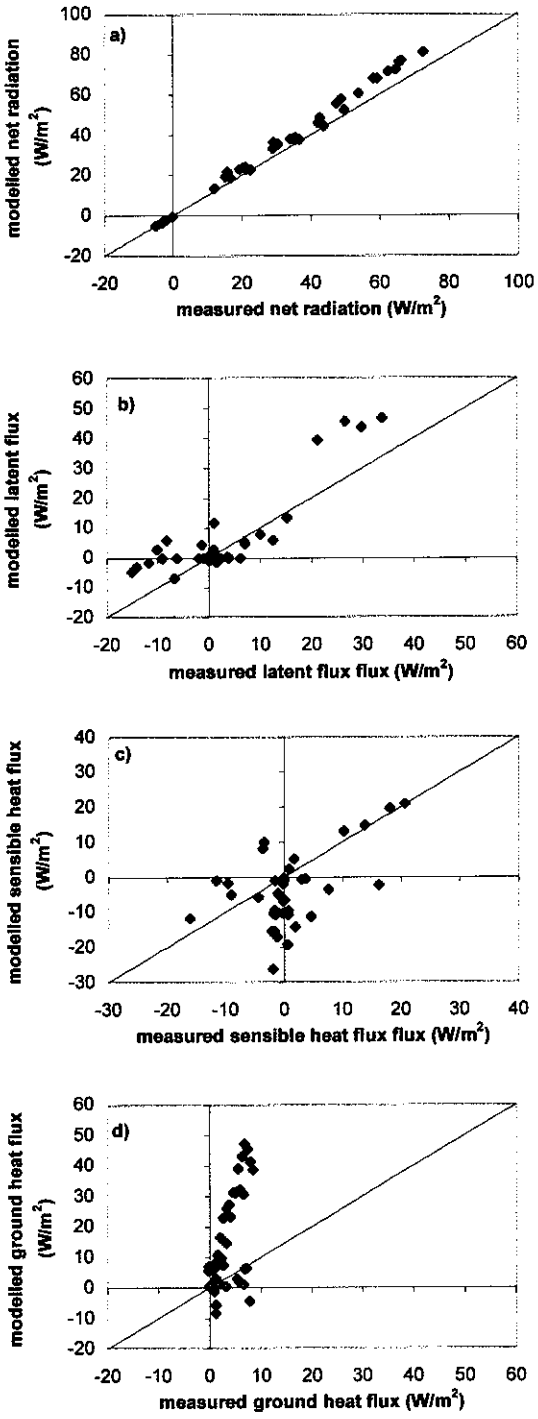

Figure 16. Comparison of 30-min fluxes for periods of melt during March 11-13, 1996, Kernan Farm near Saskatoon:

a) net radiation,

b) latent energy,

c) sensible energy, and

d) ground heat.

The data in Fig. 15a show good agreement among "modelled" and "measured" net radiation with a trend for CLASS estimates to be slightly higher than the measurements. For the three-day period, the variables showed strong correlation with a coefficient of determination $r^2 = 0.99$, a mean difference ("modelled" - "measured") equal to 4.28 W/m^2 and a standard deviation of the differences equal to 3.43 W/m^2 (see Fig. 16a). The difference is largest for high values of net radiation and may be presumed due to CLASS underestimation of snow albedo.

Figure 15b shows poorer association among the "modelled" and "measured" latent energy, compared to net radiation, but with no strong systematic trend for the CLASS values to either overestimate or underestimate the measurements. A closer inspection of the association of the latent fluxes is provided in the scatter diagram of these fluxes for the three-day period in Fig. 16b. The association has an $r^2 = 0.74$, with a mean difference equal to 2.48 W/m^2 and standard deviation of the difference equal to 6.94 W/m^2. The largest relative deviations (10-15 W/m^2) are associated with the largest latent heat fluxes (positive or negative). In other words there is a general trend for CLASS to overestimate the measured values slightly with the degree of overestimation increasing with magnitude of latent heat.

Figure 15c shows wide variations among "modelled" and "measured" sensible energy on Mar. 12/96 with small deviations during the middle parts of the period and reaching about -23 W/m^2 when melt water is generated (see Fig.14). A scatter diagram of "modelled" versus " measured" sensible energy fluxes during the three-day period for the three-day period is shown in Fig. 16c. Deviations are largest when measured sensible heat is nearly 0, but modelled sensible heat range from +2 to -28 W/m^2. The association among values has an $r^2 = 0.27$, with a mean difference of -4.48 W/m^2 and standard deviation of differences equal to 8.34 W/m^2.

Figure 15d shows that the CLASS estimates of the ground heat flux are consistently much higher than the corresponding measured value. Over the three-day period the association among variables was $r^2 = 0.34$ with a mean difference of 11.40 W/m^2 and standard deviation of differences equal to 14.94 W/m^2 (Fig.16d). On Mar. 12, the overestimation of the ground heat loss by CLASS contributed 78.2% of the shortfall in the average melt rate flux; for the three-day period it averaged 50.4% of the average melt rate flux. Such large ground heat fluxes due to heat conduction from the surface during snowmelt

infiltration into frozen mineral soils are inconsistent with the small values found by coupled heat and mass transfer theory and measurement (Zhao et al. 1997, Zhao and Gray 1997).

CONCLUSIONS

The following conclusions are made with respect to snow processes in land surface models and the identification of the next phase of improvements in these models.

1. Snow interception by forests is either neglected or grossly underestimated by land surface models but can result in substantial canopy storage of snow (up to 60% of cumulative snowfall) and latent heat flux from snow-covered canopies. A process-based snow interception model for evergreen forests based on that developed by Hedstrom and Pomeroy (1998) is able to match measured interception and should be adopted.
2. Land surface models do not characterise blowing snow redistribution and sublimation. These processes can cause substantial differences (-40% to +100% difference) between accumulated snowfall and snow accumulation in prairie and arctic regions and are necessary to include in calculations to predict mean snow water equivalent and the sub-grid variability of such.
3. With respect to snow density and snow densification it is recommended that:
   i) The density of fresh snow be calculated as a function of temperature.
   ii) The densification of well-exposed snow in areas subject to snow storms and blowing snow be treated as episodic. For non-melting snow and wind speeds greater than 7 m/s, increase snow density at a rate of 9 $kg/m^3 \cdot h$ up to a maximum that is controlled by snow depth.
   iii) For shallow, aged, wind-blown snow (mean depth, $d \leq 60$ cm) the mean density be taken equal to 250 kg/m^3 (Shook and Gray 1994). For deeper snow ($d > 60$ the average density be calculated as a function of depth.
   iv) The maximum dry snow density for forested (boreal, mountain forest, maritime) environments be set equal to 250 kg/m^3.
4. The two-parameter lognormal probability density function is recommended for describing the spatial distribution of snow water. This distribution requires knowledge of the mean and coefficient of variation of the water equivalent, CV. Initial estimates of CV can be derived from information on land cover and terrain features and the values provided in this paper.
5. Areal albedo and snow-covered area have a linear relationship during snowmelt. The snow albedo at the start of snowcover ablation should therefore not be altered during melt of the remaining snowcover. The decrease in snow-covered area can be calculated using the lognormal probability density function and an algorithm that applies calculated melt to reduce snow water equivalent and hence the area covered by snow.
6. Melt of isothermal, continuous open environment snowcovers is largely driven by radiative fluxes. Turbulent transfer schemes in land surface models will attempt to calculate a turbulent contribution to melt that is larger than necessary. A modification of the Penman equation to estimate the radiative and turbulent energy available for melt provides more accurate melt flux estimates.
7. Rapid and dramatic alterations to the soil temperature gradient during snowmelt are caused by the downward conduction of latent heat released by the refreezing of percolating meltwater. Therefore, the processes of heat and mass transfers into frozen soils during infiltration can only be described properly by a multi-layered soil model having a reasonably-small grid spacing. For those land surface models with only a few soil layers, the ground heat flux during infiltration into frozen soils should not be calculated by estimating the temperature gradient. Instead, it is likely that the assumption of a very small value for ground heat or the use of parametric or empirical correlations for estimates of both the ground heat and infiltration will give better results.
8. One land surface model, CLASS, seriously underestimated the timing and rate of snowmelt in open environments despite having relatively sophisticated snowmelt and soil routines. The exact causes of the discrepancies are unknown but it appears that overestimation of the ground heat loss during infiltration to frozen soils is a primary factor. Errors in the other energy terms for melt are compensatory and partly due to snowpack energetics, so correction of turbulent transfer and net radiation calculations in CLASS would further degrade performance. It is recommended that further study of snow energetics and soil heat conduction during infiltration of meltwater into frozen soils, be

undertaken and the results incorporated into future land surface models. It is important in this procedure to carefully establish the reliability of the models in invoking closure of the energy equation.

ACKNOWLEDGEMENTS

The assistance of Dr. Diana Verseghy in obtaining funding for this project, providing CLASS code and discussing the results is acknowledged. The authors wish to acknowledge the financial contributions of various agencies and organisations for funding that has been received in support of several studies whose results are summarised in this paper. They include: The Canadian Institute for Climate Studies, Univ. of Victoria and Environment Canada - LAND SURFACE PROCESSES and GEWEX; the Natural Science and Engineering Research Council of Canada Operating Grants, Strategic Grants and Research Partnership Program; the Canadian GEWEX program; the Prince Albert Model Forest Association Inc. and the National Hydrology Research Institute. Dr. Litong Zhao, Division of Hydrology provided many helpful discussion regarding ground heat flux and infiltration into frozen soils. The authors also wish to recognise the substantial contribution to this study of field data collected by various individuals at the Division of Hydrology and National Hydrology Research Institute over several decades with particular reference to Mr. Dell Bayne who collected and collated the data over the complete period of study.

REFERENCES

Benson, C.S., 1982. Reassessment of winter precipitation on Alaska's Arctic slope and measurements on the flux of wind-blown snow. *Geophysical Institute Report UAG R-288*. Geophysical Institute, University of Alaska, Fairbanks, 26 p.

Betts, A.K., J.H. Ball, A.C.M. Beljaars, M.J. Miller and P.A. Viterbo, 1996. The land surface-atmosphere interaction: a review based on observational and global modelling perspectives. *Journal of Geophysical Research*, 101(D3):7209-7225

Brown, T. and J. W. Pomeroy, 1989. A blowing snow particle detector. *Cold Regions Sci. Technol.*, 16:167-174.

Cess, R.D. and 32 others. 1991. Interpretation of snow-climate feedbacks as produced by 17 general circulation models. *Science*, 253:888-892.

Chow, V.T., 1954. The log-probability law and its engineering applications. *Proc. Am. Soc. Civil Eng.*, 80(536):1-25.

de La Casiniere, 1974. Heat exchange over a melting snow surface. *J. Glaciol*, 13(67):5-72.

Donald, J.R. 1992. Snowcover depletion curves and satellite snowcover estimates for snowmelt runoff modelling. PhD Thesis, Univ. of Waterloo, Waterloo, Ontario. 232 p.

Donald, J.R., E. D. Soulis, N. Kouwen and A. Pietroniro 1995. A land cover-based snow cover representation for distributed hydrological models. *Water Resources Research*, 31(4):995-1009.

Douville, H., J-F. Royer and J-F. Mahfouf, 1995. A new snow parameterization for the Meteo-France climate model, I, validation in stand-alone experiments. *Climate Dynamics*, 12:21-35.

Dyunin, A. K., 1959. Fundamentals of the theory of snow drifting. *Izvest. Sibirsk, Otdel. Akad. Nauk. USSR* No. 12:11-24. [English translation by G. Belkov, National Research Council of Canada, Ottawa, Technical Translation 952, 1961].

Essery, R.H.L. 1997. Seasonal snow cover and climate change in the Hadley Centre GCM. *Annals of Glaciology*, 25:362-366.

Goodison, B.E., H.L. Ferguson and G.A. McKay, 1981. Measurement and Data Analysis. In *Handbook of Snow: Principles, Processes, Management and Use* (eds. D.M. Gray and D.H. Male). Pergamon Press, NY, pp 191-274.

Goodison, B.E., J.R. Metcalfe, and P.Y.T. Louie, 1997. Annex 5 National Reports Of Analysis And Results. Annex 5A: Canada. In *The WMO Solid Precipitation Measurement Intercomparison Final Report*. WMO, Geneva. 15 p., in press.

Granger, R.J., 1977. Energy Exchange During Melt of a Prairie Snowcover. M.Sc. Thesis, University of Saskatchewan, Saskatoon, SK. 122 p.

Granger, R. J., and D. H. Male. 1978. Melting of a prairie snowpack. *Journal of Applied Meteorology*, 17:1833-1842.

Gray, D.M. 1970. Snow hydrology of the prairie environment. *Snow Hydrology, Proceedings of the Workshop Seminar.* Ottawa, Queen's Printer for Canada, pp.21-34.

Gray, D.M. and R.J. Granger. 1988. Bad Lake Watershed: 1967-1986. In *Proceedings of the Canadian Hydrology Symposium No. 17: Canadian Research Basins, Successes, Failures and Future.* National Research Council of Canada, Associate Committee on Hydrology. NRCC No. 30416, Ottawa, pp.143-154.

Gray, D.M. and others, 1979. Snow accumulation and distribution. In *Proc. Model. Snow Cover Runoff* (eds. S.C. Colbeck and M. Ray). US Army Cold Reg. Res. Lab., Hanover, NH, pp. 3-33.

Gray, D.M., D.I. Norum and G.E. Dyck. 1970. Densities of prairie snowpacks. *Proc. 38th Annual Meet. Western Snow Conf.*, pp.24-30.

Gray, D.M., P.G. Landine and R.J. Granger. 1985. Simulating infiltration into frozen Prairie soils in streamflow models. *Canadian Journal of Earth Sciences*, 22:464-472.

Gray, D.M. and T. Prowse, 1993. Snow and Floating Ice. In *Handbook of Hydrology* (ed. D.R. Maidment). McGraw-Hill Inc., New York, pp.7.1-7.58.

Halberstram, I. and J.P. Schieldge. 1981. Anomalous behaviour of the atmospheric surface over a melting snowpack. *J. Appl. Meteorol.*, 20:255-265.

Harding, R.J. and J.W. Pomeroy. 1996. The energy balance of the winter boreal landscape. *Journal of Climate*, 9:2778-2787.

Hedstrom, N. and J.W. Pomeroy, 1998. Intercepted snow in the boreal forest: measurements and modelling. *Hydrological Processes*, in press.

Hetherington, E.D. 1987. The importance of forests in the hydrological regime. In *Canadian Aquatic Resources* (eds. M.C. Healy and R.R. Wallace). Ottawa, Dept. of Fisheries and Oceans, pp.179-211.

Jones, H.G. 1987. Chemical dynamics of snowcover and snowmelt in a boreal forest. In *Seasonal Snowcovers: Physics, Chemistry, Hydrology* (eds. H.G. Jones and W.J. Orville-Thomas), NATO ASI Series C(211). Dordrecht, Reidel Publishing, pp.531-574.

Kane, D.L. and J. Stein. 1983. Water movement into seasonally frozen soils. *Water Resources Research*, 19(6):1547-1557.

Karl, T.R., P. Ya. Groisman, R.W. Knight and R.R. Heim. 1993. Recent variations of snow cover and snowfall in North America and their relation to precipitation and temperature variations. *Journal of Climate*, 6:1327-1344

Li, L. and J.W. Pomeroy. 1997a. Estimates of threshold wind speeds for snow transport using meteorological data. *Journal of Applied Meteorology*, 36(3):205-213.

Li, L and J.W. Pomeroy, 1997b. Probability of occurrence of blowing snow. *Journal of Geophysical Research*, 102 (D18):21955-21964.

Liston, G.E. 1995. Local advection of momentum, heat and moisture during the melt of patchy snowcovers. *Journal of Applied Meteorology*, 34(7):1705-1715.

Loth, B., H-F Graf and J.M. Oberhuber, 1993. Snow cover model for global climate simulations. *Journal of Geophysical Research*, 98:10451-10464.

Lundberg, A. and S. Halldin, 1994. Evaporation of intercepted snow: analysis of governing factors. *Water Resources Research*, 30(9):2587-2598.

Male, D.H., 1980. The Seasonal Snowcover. In *Dynamics of Snow and Ice Masses* (ed. S.C. Colbeck). Academic Press, NY, pp.305-395.

Male, D.H. and D.M. Gray, 1981. Snowcover ablation and runoff. In *Handbook of Snow: Principles, Processes, Management & Use* (eds. D.M. Gray and D.H. Male). Pergamon Press, Toronto, pp.360-436.

Male, D.H. and R.J. Granger, 1979. Energy mass fluxes at the snow surface in a Prairie environment. In *Proc. Modelling Snowcover Runoff* (eds. S.C. Colbeck and M. Ray). US Army Cold Reg. Res. and Eng. Lab., Hanover, NH, pp.101-124.

Marsh, P. and M-K. Woo, 1984. Wetting front advance and freezing of meltwater within a snow cover, 1, observations in the Canadian Arctic. *Water Resources Research*, 20(12):1853-1864.

Marsh, P. and J.W. Pomeroy, 1996. Meltwater fluxes at an arctic forest-tundra site. *Hydrological Processes*, 10:1383-1400.

Marsh, P., J.W. Pomeroy and N. Neumann, 1997. Sensible heat flux and local advection over a heterogeneous landscape at an Arctic tundra site during snowmelt. *Annals of Glaciology*, 25:132-136.

Marshall, S. and R.J. Oglesby, 1994. An improved snow hydrology for GCMs. *Climate Dynamics*, 10:21-37.

McFarlane, N. A., G. J. Boer, J.-P. Blanchet and M. Lazare. 1992. The Canadian Climate Centre second generation circulation model and its equilibrium climate. *Journal of Climate*, 5:1013 - 1044.

Monteith, J.L. 1965. Evaporation and environment. In *The State and Movement of Water in Living Organisms; Proc. 19th Symp.* Soc. Exp. Biol., Cambridge University Press, London, pp.205-233.

Monteith, J.L. 1981. Evaporation and surface temperature. *Quar. J. Roy. Meteorol.* Soc., 107(451):1-27.

O'Neill, A.D.J., 1972. The energetics of shallow prairie snowcovers. Ph.D. Thesis, University of Saskatchewan, Saskatoon, SK., 197 p.

O'Neill, A.D.J. and D.M. Gray, 1973. Solar radiation penetration through snow. In *Proc. of UNESCO-WMO-IAHS Symposia on the Role of Snow and Ice in Hydrology*, 1:227-249.

Pomeroy, J.W., 1989. A process-based model of snow drifting. *Annals of Glaciology*, 13:237-240.

Pomeroy, J.W. and R.J. Schmidt, 1993. The use of fractal geometry in modelling intercepted snow accumulation and sublimation. *Proc. Joint Meet. Eastern and Western Snow Conf.*, pp.1-10.

Pomeroy, J.W. and D.M. Gray, 1995. *Snowcover Accumulation, Relocation and Management*, National Hydrology Research Institute Science Report No. 7. NHRI, Environment Canada, Saskatoon, SK, 144 p.

Pomeroy, J.W. and K. Dion, 1996. Winter radiation extinction and reflection in a boreal pine canopy: measurements and modelling. *Hydrological Processes*, 10:1591-1608.

Pomeroy, J.W. and B.E. Goodison, 1997. Winter and snow. In *The Surface Climates of Canada* (eds. W.G. Bailey, T.R. Oke and W.R. Rouse). McGill-Queen's University Press, Montreal & Kingston, pp.68-100.

Pomeroy, J.W. and R.J. Granger, 1997. Sustainability of the western Canadian boreal forest under changing hydrological conditions, I, snow accumulation and ablation. In *Sustainability of Water Resources under Increasing Uncertainty*. IAHS Publ. No. 240. Wallingford, UK, IAHS Press, pp.237-242

Pomeroy, J.W. and L. Li, 1997. Development of the Prairie Blowing Snow Model for application in climatological and hydrological models. *Proceedings of the Eastern Snow Conference*, 54:186-197.

Pomeroy, J.W., D.M. Gray and P.G. Landine. 1993. The Prairie Blowing Snow Model: characteristics, validation, operation. *Journal of Hydrology*, 144:165-192.

Pomeroy, J.W., R.J. Granger, A. Pietroniro, J. Elliott, B. Toth and N. Hedstrom. 1997a. *Hydrological Pathways in the Prince Albert Model Forest*. NHRI Contribution Series CS-97004. NHRI, Saskatoon. 154 p. + app.

Pomeroy, J.W., P. Marsh and D.M. Gray, 1997b. Application of a distributed blowing snow model to the Arctic. *Hydrological Processes*, 11:1451-1464.

Randall, D.A. and 26 others, 1994. Analysis of snow feedbacks in 14 general circulation models. *Journal of Geophysical Research*, 99:20757-20771.

Schmidt, R.J. JR., 1972. Sublimation of wind-transported snow - "A Model". *Res. Pap. RM-90*. USDA Forestry Service, Rocky Mountain Forest and range Experimental Station, Fort Collins, CO.

Schmidt, R.A. and D.R. Gluns, 1991. Snowfall interception on branches of three conifer species. *Can. J. Forest Res.*, 21:1262-1269.

Sellers, P.J. and eight others, 1996. A revised land surface parameterisation (SiB2) for atmospheric GCMs, part 1: model formation. *Journal of Climate*, 9: 676-705.

Shook, K., 1993. Fractal geometry of snowpacks during ablation. M.Sc. Thesis, Univ. Sask., Saskatoon, SK., 178 p.

Shook, K., 1995. Simulation of the Ablation of Prairie Snowcovers. Ph.D. Thesis. Univ. Sask., Saskatoon, SK., 189 p.

Shook, K. and D.M. Gray, 1994. Determining the snow water equivalent of shallow prairie snowcovers, *Proc. 51st Annual Meet. Eastern Snow Conf.*, Dearborn, MI, pp.89-95.

Shook, K. and D.M. Gray, 1997. Snowmelt resulting from advection. J. Hydrological Processes, 11:1725-1736.

Shook, K., D.M. Gray and J.W. Pomeroy, 1993. Temporal variation in snowcover area during melt in Prairie and Alpine environments. *Nordic Hydrol.*, 24:183-198.

Shook, K., D.M. Gray and J.W. Pomeroy, 1994. Geometry of patchy snowcovers. *Proc. 1993 Annual Meet. Eastern Snow Conf.* June 8-10, 1993, Quebec City, QUE., pp.89-96.

Steppuhn, H. and G.E. Dyck, 1974. Estimating true basin snowcover. In *Advanced Concepts and Tech. in the Study of Snow and Ice Resour.* Nat. Acad. Sci., Washington, DC, pp.314-328.

Sturm, M., 1992. Snow distribution and heat flow in the taiga. *Arctic and Alpine Research*, 24(2):145-152.

Tabler, R.D., J.W. Pomeroy and B.W. Santana, 1990. Drifting snow. In *Cold Regions Hydrology and Hydraulics* (eds.W.L. Ryan and R.D. Crissman). Am. Soc. Civil Eng., NY, pp.95-146.

Thomas, G. and P.R. Rowntree. 1992. The boreal forest and climate. *Quarterly Journal of the Royal Meteorological Society*, 118:469-498.

US Army Corps of Engineers, 1956. Snow Hydrology: *Summary Report of the Snow Investigations*. North Pacific Division, Portland, OR, 437 p.

Verseghy, D.L. 1991. CLASS - a Canadian land surface scheme for GCMs I. Soil model. *International Journal of Climatology*, 11:111-133.

Verseghy, D.L., N.A. McFarlane and M. Lazare. 1993. CLASS - a Canadian land surface scheme for GCMs II. Vegetation model and coupled runs. *International Journal of Climatology*, 13:347-370.

Viterbo, P. and A.C.M. Beljaars, 1995. An improved land surface parameterisation scheme in the ECMWF model and its validation. *Journal of Climate*, 8:2716-2748.

Wiscombe, W.J. and S.G. Warren, 1980. A model for the spectral albedo of snow, I, pure snow. *Journal of Atmospheric Sciences*, 37:2712-2733,

Webb, E. K. 1970. Profile relationships : The log-linear range and extension to strong stability. *Quarterly Journal of the Royal Meteorological Society*, 96:67-90.

Woo, M-K. 1990. Permafrost hydrology. In *Northern Hydrology: Canadian Perspectives* (eds. T.D. Prowse and C.S.L. Ommanney). NHRI Science Report No. 1. Saskatoon, Minister of Supply and Services Canada, pp.63-76.

Woo, M-K. and P. Marsh, 1977. Determination of snow storage for small eastern high Arctic basins, Proc. *1977 Annual Meet. Eastern Snow Conf.*, Feb. 3-4, Belleville, ON, pp.147-162.

Woo, M-K and P. Steer, 1986. Monte Carlo simulation of snow depth in a forest. *Water Resour. Res.* 22(6):864-868.

Woo, M-K., R. Heron and P. Marsh. 1982. Basal ice in high arctic snowpacks. *Arctic and Alpine Research*, 14(3):251-260.

Yen, Yin-Chao. 1995. Sensible heat flux measurements near a cold surface. *US Army Cold Regions Research and Engineering Laboratory Report* 95-22, Hanover, NH 42 p.

Zhao, L. and D.M. Gray. 1997. A parametric expression for estimating infiltration into frozen soils. *Hydrological Processes*, 11:1761-1775.

Zhao, L., D.M. Gray and D.H. Male. 1997. Numerical analysis of simultaneous heat and mass transfer during infiltration into frozen ground. *Journal of Hydrology*, 200:345-363.